Nuclear Engineering and Design 444 (2025) 114390

Contents lists available at ScienceDirect

Nuclear Engineering and Design

journal homepage: www.elsevier.com/locate/nucengdes

Modelling of decontamination factor in swarm flow based on residence times

Xu Cheng , Fanli Kong *, Xing Chen

Institute for Applied Thermofluidics (IATF), Karlsruhe Institute of Technology (KIT), Kaiserstrasse 12, 76131 Karlsruhe, Germany

ARTICLE INFO

Keywords:
Decontamination factor
Swarm flow
Residence time
Particle removal

ABSTRACT

Pool scrubbing process is an important measure to minimize the radioactive material release in the containment. Decontamination factor describes the efficiency of aerosol removal in the pool scrubbing process and requires reliable modelling and prediction. In the existing aerosol retention code, conventional approaches are applied, which rely on the deposition velocity of particles at the interfacial area. During the pool scrubbing process, both gas bubble topology and movement show a strong dynamic behaviour and cannot be well described using simple models. This leads to a big deficiency in reliable modelling of the decontamination factor. To overcome this difficulty, a new approach is introduced in this paper to model the decontamination factor based on the statistical treatment of the residence time of bubbles in the liquid pool as well as the residence time of particles inside bubbles. Two different groups of CFD simulations are carried out to investigate the bubble behaviour in the water pool and the particle transportation inside bubbles, respectively. The numerical results achieved so far indicate that the probability density functions of both bubble removal and particle removal can be well represented with simple exponential decay functions. Thus, the good feasibility of the new modelling approach is successfully confirmed.

1. Introduction

During a severe accident (SA) in nuclear power plants with water cooled reactors, radioactive aerosols escape from the molten fuel in the primary loop, where they are mixed with water and non-condensable gases and released into the containment or in a foreseen water pool. When the gas mixture goes through a water pool, part of the aerosol particles will be washed down and remain in the water pool. The rest aerosol particles escape into the gas room of the containment. This process is called pool scrubbing. The parameter decontamination factor (DF) is introduced to quantify the efficiency of the wash down process and defined as the ratio of the aerosol mass entering the water pool to the aerosol mass leaving the water pool (Herranz et al., 1996):

$$DF = \frac{m_{\text{in}}}{m_{\text{out}}} \tag{1}$$

Fig. 1 shows schematically the important patterns in a pool scrubbing process. During a pool scrubbing process, flow can be divided into three regions, i.e. injection region, transition region and swarm flow region. As the gas mixture is injected into the water pool, large gas bubbles are formed, also called globules. In their rising paths, globules break up into small bubbles. This happens in the transition region, which takes normally a short distance. In the following swarm flow region, bubbles with small diameters (swarm bubbles) rise upward, reach the upper surface of water pool and, subsequently, escape from the water pool.

The swarm flow is characterized with 3-dimensional natural circulation with recirculation zones, driven by drag force and buoyancy force. Studies showed that the particle removal in the swarm flow region plays the most important role in the entire pool scrubbing process (Lee and Cho, 2019). In general, the decontamination factor of particles inside a bubble with surface area A and volume V can be analytically determined by the following equation:

$$DF = e^{\left\{\frac{1}{V}\bullet\int_0^{\tau}\int_A \max\{u_n-u_C,0\}\bullet dA\bullet dt\right\}} \tag{2}$$

Here u_n is the normal velocity directed to the interface, u_C is the critical normal velocity, above which particle can penetrate the liquid. The main difficulty in calculating the decontamination factor is the determination of the normal velocity of the particle at the interface. In the swarm flow region, two extremely challenging issues need to be addressed. Firstly,

* Corresponding author.
E-mail address: fanli.kong@kit.edu (F. Kong).

https://doi.org/10.1016/j.nucengdes.2025.114390
Received 10 January 2025; Received in revised form 12 June 2025; Accepted 8 August 2025
Available online 16 August 2025

Nomenclature

A	bubble surface area (m^2)
a	major axis of elliptic bubble (m)
$A_{cell,j}$	cell area in each cell (m^2)
b	minor axis of elliptic bubble (m)
BDF	bubble deformation factor (−)
C_{mi}	correction factor (−)
C_{ni}	cunningham slip correction factor (−)
CPD	cells per bubble diameter (−)
D	pool diameter (m)
D_B	bubble diameter (m)
D_e	equivalent diameter (m)
D_i	diffusion coefficient (−)
d_P	particle diameter (m)
DF	decontamination factor (−)
$\mathbf{F}_B$	additional forces for discrete bubble (kg • m/s^2)
F_i	probability of bubbles in group i (−)
$\mathbf{g}, g$	gravitational acceleration (m/s^2)
H	pool height (m)
h	water depth (m)
h_0	submergence height (m)
h_{in}	injection height (m)
k_B	Boltzmann constant (−)
M	total number of data points (−)
m_B	mass of bubble (kg)
$\dot{m}_j$	air mass flow rate in each cell (kg/s)
m_{in}	aerosol mass entering the water pool (kg)
m_{out}	aerosol mass leaving the water pool (kg)
N	particle number (−)
N_0	initial total particle number (−)
N_j	equivalent bubble number of each cell (−)
P_B	probability density function for bubble removal (s^{-1})
P_P	probability density function for particle removal (s^{-1})
$\dot{Q}$	gas volume flow rate (L/s)
r_c	surface radius of curvature (m)
RR	removal ratio (−)
T	absolute temperature (K)
t_e	exposure time of the moving surface (s)
u	effective rising velocity of bubbles (m/s)
u_B	velocity contribution from Brown diffusion (m/s)
$\mathbf{u}_B$	bubble velocity vector (m/s)
u_C	critical normal velocity (m/s)
u_c	velocity contribution from centrifugal deposition (m/s)
u_g	velocity contribution from gravitational sedimentation (m/s)
u_n	normal velocity directed to the interface (m/s)
$u_{P,n}$	normal velocity of the particle relative to the interface (m/s)
u_s	local surface velocity (m/s)
u_v	velocity contribution from phase change (m/s)
$\mathbf{u}_w$	water velocity vector (m/s)
V	bubble volume (m^3)
w_g	z-velocity of air in the global coordinate system (m/s)
We	Weber number (−)
We_c	critical particle Weber number (−)
We_P	particle Weber number (−)
x_{nc}	mass fraction of non-condensable gases (−)

Greek symbols

α_B	decay constant for bubble removal (s^{-1})
α_g	void fraction (−)
α_P	decay constant for particle removal (s^{-1})
μ	gas dynamic viscosity (kg/(m • s))
ρ_g	air density (kg/m^3)
ρ_B	bubble density (kg/m^3)
ρ_P	particle density (kg/m^3)
ρ_w	water density (kg/m^3)
σ	surface tension (N/m)
τ	bubble residence time (s)
τ_r	relaxation time (s)

Subscripts

i	size group of swarm bubbles (−)
j	cell index (−)

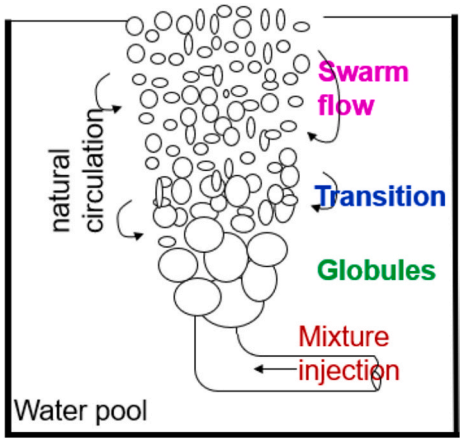

Fig. 1. Important flow patterns in a pool scrubbing process.

the movement of particles inside gas bubbles and their removal at the interfacial area. Various phenomena make contribution to the particle removal, e.g. centrifugal deposition, gravitational sedimentation, phase change and diffusion (Mei and Cheng, 2023). An accurate description of particle movement is the pre-condition to analyse the particle deposition behaviour. Secondly, the dynamic behaviour of the gas–liquid interface, where particle deposition happens. In the rising process, the movement and topology of swarm bubbles don't show stationary behaviour and vary strongly during the rising process (Mei and Cheng, 2024). Thus, the normal velocity relative to the interface also shows non-stationary behaviour. Thus, it is extremely difficult, or even impossible, to use Eq. (2) for the determination of the decontamination factor.

The main objective of this study is to develop a new methodology for modelling decontamination factor. Instead of modelling all parameters in Eq. (2), the new methodology uses residence time of both bubbles in pool and particles in bubbles, to avoid the modelling of the dynamic behaviour of interfacial surface. In Section 2, both the existing and the new developed methodologies are presented. Numerical models used for single bubble dynamics as well as swarm flow are explained in Section 3. Preliminary results achieved so far are presented in Section 4, to confirm the feasibility of the new methodology.

2. Modelling methodologies

To justify the importance and necessity of the development of the new methodology, the existing, conventional methodology of calculating the decontamination factor is presented first.

2.1. Existing methodology

In the containment safety analysis programs, the aerosol retention models are applied, to calculate the decontamination factor. Intensive investigations in the 1980's led to the development of several aerosol retention code, such as SPARC (Suppression Pool Aerosol Removal Code) from Pacific Northwest National Laboratory (Owczarski and Burk, 1991) and BUSCA (BUbble Scrubbing Algorithm) from the United Kingdom (Ramsdale et al., 1995). Both codes were widely applied in the community, have a similar approach to determine the decontamination factor and use Eq. (2) as a starting point.

The size of swarm bubbles is divided into several groups, indicated with the subscript *i*. The decontamination factor of group *i* is determined similar to Eq. (2), i.e.

$$DF_i = e^{\left\{\frac{1}{V_i}\bullet\int_0^{\tau}\int_{A_i} u_{n,i}\bullet dA\bullet dt\right\}} \tag{3}$$

where τ is the bubble residence time in the water pool. Compared to Eq. (2), the critical velocity is set to zero in the conventional applications. That means, as soon as particles arrive at the interface, they will deposit on the interface and penetrate the liquid. The entire decontamination factor is determined by

$$DF = \frac{1}{\sum_i \frac{F_i}{DF_i}} \tag{4}$$

with F_i the probability of bubbles in group *i*. It can be recognized that the decontamination factor depends not only on the bubble behaviour such as bubble geometry and bubble residence time, but also on the particle behaviour inside the bubble, e.g. the interfacial deposition velocity $u_{n,i}$. During the bubble rise, the net deposition velocity $u_{n,i}$ is calculated by summing the contributions from different mechanisms:

$$u_{n,i} = u_{B,i} + u_{g,i}cos\beta + u_{c,i} - u_{v,i} \tag{5}$$

Eq. (5) considers four different processes, i.e. Brown diffusion u_B, gravitational sedimentation u_g, centrifugal deposition u_c and phase change (incoming vapor velocity) u_v. β is the angle between the local interfacial normal vector and the vertical direction (gravity). Furthermore, it was found that in most cases the centrifugal deposition plays the most important role.

The total decontamination factor is the product of all individual contributions, i.e.

$$DF_i = DF_i\left(u_{B,i}\right)\bullet DF_i\left(u_{g,i}\right)\bullet DF_i\left(u_{c,i}\right)\bullet DF_i\left(u_{v,i}\right) \tag{6}$$

In SPARC (Owczarski and Burk, 1991), various terms are calculated as below:

- Gravitational sedimentation velocity $\left(u_{g,i}\right)$

$$u_{g,i} = \frac{\rho_P \bullet d_P^2 \bullet g \bullet C_{ni}}{18\mu} \tag{7}$$

where C_{ni} is the Cunningham slip correction factor.

- Centrifugal deposition velocity $\left(u_{c,i}\right)$

$$u_{c,i} = \frac{u_s^2 \bullet u_{g,i}}{r_c g} \tag{8}$$

where u_s is local surface velocity and r_c is surface radius of curvature.

- Brownian diffusion velocity $(u_{B,i})$

According to penetration theory of mass transfer (Crank. 1979), the local Brownian diffusion velocity $u_{B,i}$ is estimated as:

$$u_{B,i} = \left(\frac{D_i}{\pi t_e}\right)^{1/2} \tag{9}$$

where D_i is the diffusion coefficient and can be calculated using the Stokes-Einstein equation

$$D_i = \frac{k_B T C_{mi}}{\pi d_P \mu} \tag{10}$$

where k_B is Boltzmann constant, T is absolute temperature, C_{mi} is correction factor, d_P is particle diameter and μ is viscosity of the medium. t_e relates to the exposure time of the moving surface.

Although the above sub-models have been used in engineering applications, the reliability is very questionable. One of the main challenges is the dynamic feature of the bubble parameters such as bubble shape, bubble velocity and subsequently the interfacial surface. This makes a reliable deterministic description of the interfacial surface hardly possible. The deposition velocity is the relative velocity of particles to the interfacial surface. Thus, it is also hardly possible to quantitatively describe the deposition velocity. Furthermore, the four terms of deposition velocity cannot be separately determined in experiments. Thus, there is a big deficiency in experimental validation of the sub-models.

In addition, the geometric parameters of bubble as well as its residence time τ are required to determine the decontamination factor as seen in Eq. (3). In the aerosol retention code SPARC, it is assumed that swarm bubbles have the elliptic shape, as indicated in Fig. 2.

The equivalent diameter is determined by

$$D_e = 0.0072e^{\left(2.303\left(-0.2265+(0.0203+0.0313x_{nc})^{0.5}\right)\right)} \tag{11}$$

The ratio of both axes is

$$\frac{b}{a} = 0.8407 + 1.13466 \bullet D_e - 0.3795 \bullet D_e^2 \tag{12}$$

The effective rising velocity of bubbles is given by

$$u = \left(\frac{\left(\dot{Q}+5.33\right)\bullet 10^{-3}}{3.011}\right)^{0.5}\left(1 - 3.975 \bullet 10^{-2} \bullet h\right) \tag{13}$$

From the effective rising velocity, the residence time of bubbles is given as

$$\tau = \int_0^h \frac{dz}{u} \tag{14}$$

In the above equations, $\dot{Q}$ is gas volume flow rate, h is the water depth and x_{nc} is the mass fraction of non-condensable gases.

Because of the deficiency in reliably validated sub-models for the particle deposition velocities and residence time, the feasibility and accuracy of the conventional aerosol retention models are questionable. Furthermore, it was found that aerosol retention models used in different codes give significant derivation from each other and none of them were well approved or sufficiently validated (Herranz and Sánchez, 2019).

Therefore, in the present paper, a new methodology to calculate the decontamination factor is developed, instead of the conventional methodology based on Eq. (3).

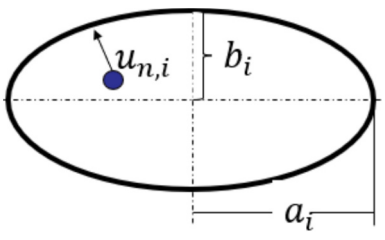

Fig. 2. Elliptic bubble assumed in SPARC code.

2.2. New modelling methodology

As discussed in the previous section, although the conventional methodology based on Eq. (3) was derived analytically, reveals enormous difficulty because of the dynamic feature of the hydrodynamic parameters.

The new methodology focuses on the statistic treatment of the residence times of both the bubble in the water pool and the aerosol particles inside a bubble. To explain the new methodology, probability density functions (PDFs) for both the bubble removal $P_B(\tau)$ and the particle removal $P_P(t)$ are introduced. By knowing both PDFs, probability of bubbles remaining in the pool after time t is

$$1 - \int_0^t P_B(\tau) \bullet d\tau \tag{15}$$

In the following time interval $\{t,\ t+\delta t\}$, the removed particle portion is determined by

$$\left\{1 - \int_0^t P_B(\tau) \bullet d\tau\right\} \bullet P_P(t)dt \tag{16}$$

The total particle portion, which is removed in the period $\{0,\ T\}$ yields

$$RR(T) = \int_0^T \left\{1 - \int_0^t P_B(\tau) \bullet d\tau\right\} \bullet P_P(t)dt \tag{17}$$

RR is called removal ratio in this paper. The entire decontamination factor can be easily derived from the removal ratio as

$$DF = \frac{1}{1 - RR(\infty)} = \frac{1}{1 - \int_0^\infty \left\{1 - \int_0^t P_B(\tau) \bullet d\tau\right\} \bullet P_P(t)dt} \tag{18}$$

In case the particle size is divided into sub-groups, the decontamination factor for each group i is

$$DF_i = \frac{1}{1 - RR_i(\infty)} = \frac{1}{1 - \int_0^\infty \left\{1 - \int_0^t P_{B,i}(\tau) \bullet d\tau\right\} \bullet P_{P,i}(t)dt} \tag{19}$$

The total decontamination factor is then calculated using Eq. (4).

From Eqs. (18) or (19), it is recognized that the decontamination factor can be easily determined by knowing both PDFs $P_{B,i}(\tau)$ *and* $P_{P,i}(t)$. The main focus is put on the development of models for both PDFs.

The expected probability density function of bubble removal in water pool is schematically illustrated in Fig. 3.

The entire behaviour can be divided into three parts. In the time range $(0, t_1)$, no bubble escapes from the water pool, because the bubble needs time to arrive at the surface. Obviously, the time point t_1 depends on the submerged height of water pool. In the second time interval (t_1, t_2), the PDF increases and reaches its maximum. The time point with maximum probability t_2 is strongly related to the average bubble rising velocity. In the third zone, a monotonous decrease in the probability density function is expected. Due to flow recirculation in the water pool, some bubbles can stay in the pool for long time.

The probability density function of the removal of particles inside bubble is qualitatively shown in Fig. 4. Surely, it would differ strongly from that of bubbler removal behaviour in the pool. Due to the decrease of particle number with time, the removed particle number for the same time interval becomes also smaller. Thus, the PDF decreases continuously. Assuming, that the bubble doesn't change its shape, particles have uniform distribution inside the bubble and the same velocity, the particle removal rate can be expressed by

$$\frac{dN}{dt} = -N \bullet \frac{1}{V}\int_A max\{u_n - u_C, 0\} \bullet dA = -N \bullet \alpha_P \tag{20}$$

with

$$\alpha_P = \frac{1}{V}\int_A max\{u_n - u_C, 0\} \bullet dA \tag{21}$$

Under the simplified assumption that α is time independent, solution of Eq. (20) yields

$$N(t) = N_0 \bullet e^{-\alpha_P t} \tag{22}$$

The probability density function is derived as

$$P_P(t) = -\frac{1}{N_0} \bullet \frac{dN}{dt} = \alpha_P e^{-\alpha_P t} \tag{23}$$

Under the above strong simplification, it indicates that the PDF, $P_P(t)$, might be well correlated with an exponential decay function.

To investigate the behaviour of both PDFs, $P_B(\tau)$ *and* $P_P(t)$, CFD simulations have been carried out in two individual groups. In the first group particle transportation in a single swarm bubble is simulated to statistically find out the residence time of particles, whereas the second group is devoted to swarm flow with the focus on the statistic investigation of bubble residence time.

3. Numerical approaches

For numerical simulation, the open source CFD platform OpenFOAM is used. Different numerical approaches are applied to swarm flow and single bubble flow, respectively.

3.1. Single bubble and particle transportation

The VOF-LPT (Volume of Fluid & Lagrangian Particle Tracking) method is used for this purpose. It is a one-way coupling approach that utilizes the VOF method to capture the gas–liquid interface and the LPT method to track aerosol particles. The combination of the VOF and LPT methods provides a detailed description of bubble dynamics and particle transport, offering insights into the mechanisms of particle removal at the gas–liquid interface.

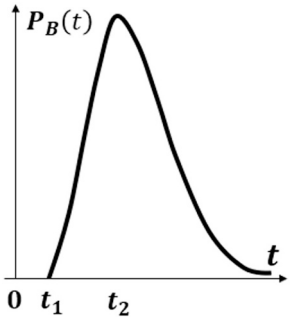

Fig. 3. PDF of bubble removal.

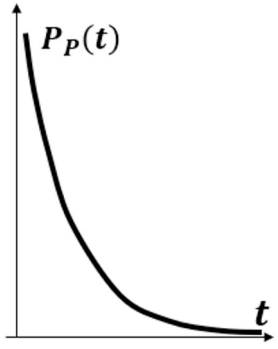

Fig. 4. PDF of particle removal.

The computational domain has a square cross-section with the side length $5D_B$ and the height $20D_B$, where D_B refers to bubble equivalent diameter, as shown in Fig. 5. In the beginning, the bubble is assumed to be spherical, and it is put along the central axis with a height $5D_B$.

To track the long-term bubble and aerosol behaviours, the computational domain is moving along the z direction and its velocity is set to be equal to the bubble terminal velocity roughly. Evaluation is carried out to assess the effect of mesh structure and various schemes for the suppressing interfacial diffusion. The numerical models and the corresponding validation compared with experimental data (Fujiwara et al., 2022) have been described in detail in the previous publications (Mei and Cheng, 2022; Mei et al., 2022; Mei and Cheng, 2023). In the following, only important aspects related to particle injection and particle deposition are briefly summarized.

During the initial phase of bubble rise, it was observed that the bubble deformation exhibited irregularities, during the first second, shown as in Fig. 6. The bubble deformation factor (BDF) which is defined as the ratio of the actual three-dimensional surface area of the bubble to that of an equivalent spherical bubble, has severe fluctuations at the beginning and tends to approach the terminal condition in about 1 s. Thus, in the present study, particle injection is initiated 1 s after bubble starts to rise.

Initially, the bubble was configured as spherical and allowed to rise freely for one second. After this period, the deformed bubble shape was extracted, and the center coordinates of each mesh element within the bubble were identified. Subsequently, a large number of particles, e.g. one million particles, are randomly injected into the mesh of the current bubble shape.

The motion of aerosol particles is governed by Newton's motion equation which the drag force, gravity force, buoyance force and Brownian force are considered within the resolved flow field obtained through the VOF method at each time step.

Due to the significantly smaller size of aerosol particles compared to the bubble diameter, the volume they occupy and their effect on the internal flow field are neglected. In other words, the temporal evolution of the fluid phase influences the particle phase, but not the other way around.

As mentioned in Eq. (2), particles, which reach the interface, do not necessarily deposit on the interface and penetrate the liquid. Penetration happens only if their normal velocity is larger than the critical value or the Weber number is larger than the critical Weber number, see Eqs. (24) and (25). Thus, in the present study, a flow chart to judge the movement of particles near the interface is introduced and presented in Fig. 7. The value of void fraction is used to identify whether a particle locates near the interface. If the void fraction is larger than 90 % ($\alpha_g \geq 90\%$), the particle is assumed to be in the gas phase and far from the interface, whereas in case the void fraction is smaller than 10 % ($\alpha_g \leq 10\%$), the particle locates inside the liquid water. Only if the void fraction is in the range of $10\% \leq \alpha_g \leq 90\%$, the particle is assumed to be near the interface. In this case, the critical Weber is applied to judge whether this particle penetrates into the liquid water ($We_P > We_c$) or rebound from the interface back to the gas phase ($We_P \leq We_c$).

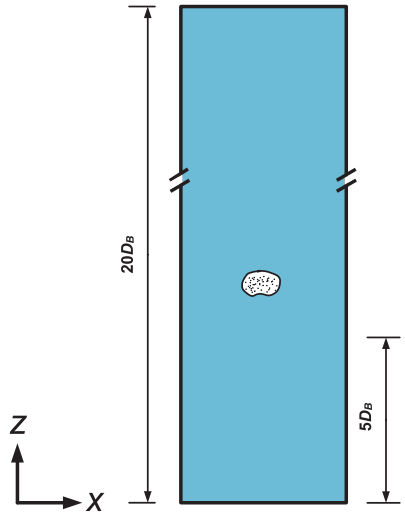

Fig. 5. Schematic of a bubble with internal aerosol rising in quiescent liquid.

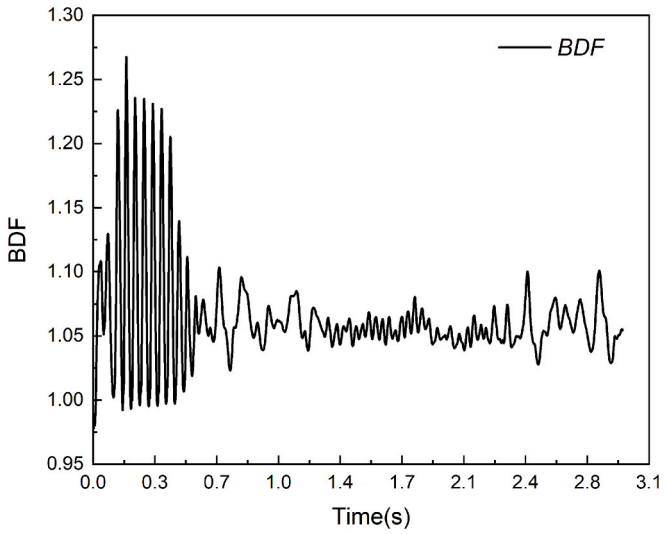

Fig. 6. Temporal evolution of bubble deformation factor (Mei and Cheng, 2022).

As investigated in the previous publication (Mei and Cheng, 2023), an interfacial penetration model is derived from the theoretical analysis and the criterion with critical Weber number was introduced and assessed based on the experimental data. The Weber number is defined as

$$We_p = \frac{\rho_p \bullet d_p \bullet u_{p,n}^2}{\sigma} \tag{24}$$

Comparison with experimental data (Fujiwara et al., 2020) determined the critical Weber number as

$$We_C = 3.0 \bullet 10^{-4} \tag{25}$$

3.2. Numerical approach for swarm flow

Fig. 8 shows the approach selected for the simulation of swarm flow. The two-fluid Euler-Euler method is selected for the bubbly two-phase flow region, which is different from the VOF method used in single bubble simulation considering the computational cost and experiences from other literatures (Bicer et al., 2021; Liao et al., 2022). After the time-averaged two-phase flow field is obtained, the Lagrangian model is applied to describe the bubble trajectory. One-way coupling is utilized in this work, that is, the flow affects the bubble motion, but the effect of air bubbles on the water flow field was not involved in the Lagrangian part since the air–liquid flow has been simulated by Euler-Euler approach. From the trajectory results of many bubbles, statistical results of bubble residence time are obtained.

The whole computational domain, as shown in Fig. 9, is cylinder and has the dimension $D \times H = 0.5\ \text{m} \times 3.5\ \text{m}$. The submergence height h_0 is 3 m. The air injection cross-section locates at height $h_{in} = 0.3$ m from the water pool bottom. The nozzle is a rectangular section, whose area is varied to keep the air inlet velocity equal to 0.5 m/s. The air–water two-phase flow is assumed as the monodispersed flow and the constant bubble diameter is set in simulation. The total physical time is set as 30 s. The results in the time interval from 15 s to 30 s are used for calculating

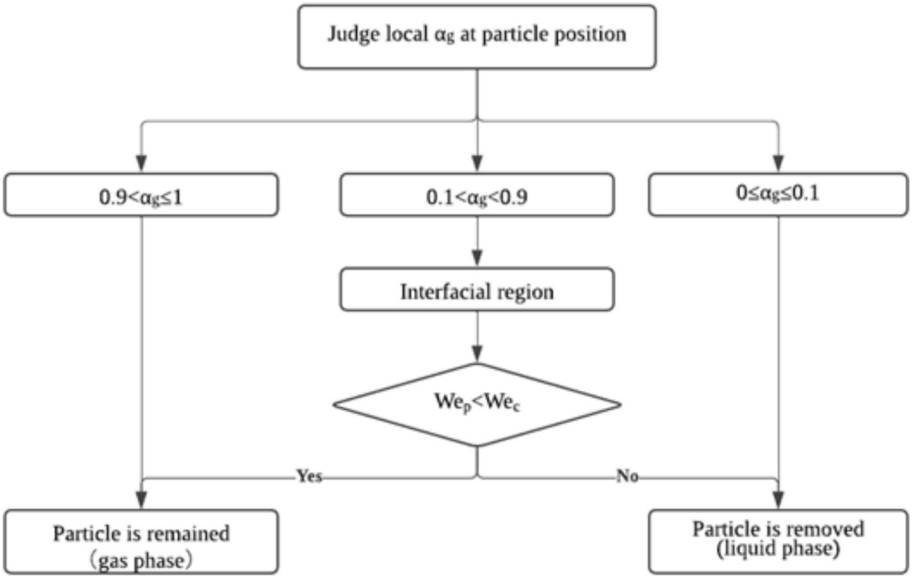

Fig. 7. Flow chart of the simulation process (Mei and Cheng, 2023).

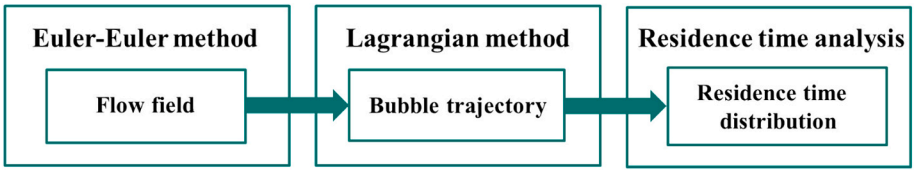

Fig. 8. Numerical approach for determination of bubble residence time.

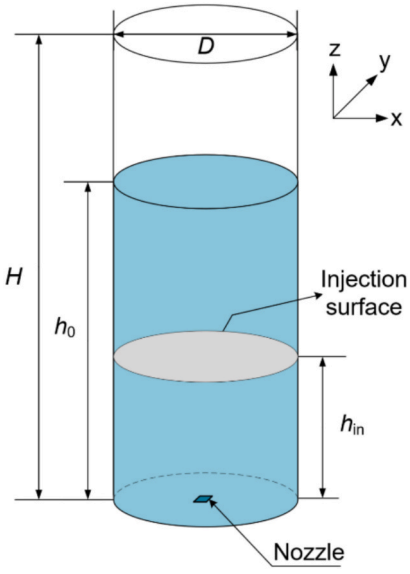

Fig. 9. Schematic diagram of computational domain.

the average results.

The interface momentum transfer in Euler-Euler approach includes the drag force, lift force, virtual mass force, turbulent dispersion force and wall lubrication force. All the selections of the interfacial force models and turbulence modeling are referred to the baseline model (Hänsch et al., 2021), as also documented in the previous publication (Kong and Cheng, 2025). The Euler-Euler model has been well validated with the experimental data of Abe et al. (2018) and can be found in Kong and Cheng (2025).

The bubble transportation as dispersed phase is solved in a Lagrangian reference system. The force balance equation of a discrete bubble is written as:

$$m_{\mathrm{B}}\frac{d\mathbf{u}_{\mathrm{B}}}{dt}=m_{\mathrm{B}}\frac{\mathbf{u}_w-\mathbf{u}_{\mathrm{B}}}{\tau_r}+m_{\mathrm{B}}\frac{\mathbf{g}(\rho_{\mathrm{B}}-\rho_w)}{\rho_{\mathrm{B}}}+\mathbf{F}_{\mathrm{B}} \tag{26}$$

where the subscripts B and w denote bubble (the discrete phase) and water phase (the carrier phase), m_B is the mass of bubble and τ_r is the relaxation time. The terms on the right side are the drag force (the first term), the combined force of gravity and buoyancy (second term), and $\mathbf{F}_{\mathrm{B}}$ (third term) denotes the lift force, virtual mass force, and pressure gradient force which are considered in this work. To keep consistence with the Euler-Eulerian approach, the same models for various forces in the above bubble transportation equation were used as in the Euler-Eulerian two fluid approach. The specific numerical settings of Lagrangian approach are referred to the previous work (Kong and Cheng, 2025).

To investigate bubble residence time in the swarm region, the discrete bubbles are injected from each cell center of the injection cross-section (the gray plane shown in Fig. 9). Bubbles are removed from the computational domain, when they reach the initial water surface, and considered as leaving from the pool. Each bubble represents a group of bubbles injected in the same cell. The discrete phase consists of air bubbles and their properties and velocities on the injection cross-section are obtained from the Euler-Eulerian simulation. The air mass flow rate in each cell could be calculated as:

$$\dot{m}_j = w_g\alpha_g\rho_g A_{cell,j} \tag{27}$$

where w_g is the air vertical velocity, α_g the void fraction, ρ_g the air density, and $A_{cell,j}$ the cell area. After that, the equivalent bubble number

of each cell could be converted from the mass flow rate:

$$N_j = \frac{6\dot{m}_j}{\pi d^3 \rho_g} \tag{28}$$

4. Results and discussion

This section presents the results obtained so far into two parts, i.e. (a) particle transportation and residence time, (b) swarm flow and bubble residence time.

4.1. Particle transportation and residence time

The dynamics of single bubble was intensively investigated and documented in Mei and Cheng (2022). As example, the temporal evolution of bubble shape and internal flow field is shown in Fig. 10, labeled from 1 to 10 in a sequential manner. Initially, the bubble shape appears as a flattened oblate form. In presence of a large bubble front surface contacting with liquid water, the pressure drag force on the bubble is relatively large, resulting in the deceleration in bubble velocity in the time sequences from 1 to 3. Concurrently, since the bubble presents a highly deformed shape at the starting point, the large interface curvature results in a dominant surface tension force on the bubble, which contributes to the bubble shape relaxing to the initial round shape embodied in the time sequences from 1 to 6. Furthermore, given that the contacting area between air and water is decreased in the shape relaxation process, the bubble buoyancy force is more predominant than the drag force and consequently, the bubble accelerates and the peak comes at sequence 7. At this specific time point, the bubble presents a nearly round shape and the highest local rising velocity. After that, further shape deformation occurs, which is followed by the deceleration of bubble rising velocity in the time sequences from 8 to 10. The example of results shows clearly the dynamic behaviour of bubble, especially its topology and interfacial boundary area.

Following parameters are taken into variation to study their effect on the particle deposition behaviour, i.e.

- bubble size, [mm]: 4.0, 6.0, 9.0
- particle size, [μm]: 0.5, 1.0, 2.0
- particle density, $[kg/m^3]$: 1000, 1500, 2000
- surface tension of water, [N/m]: 0.04, 0.07, 0.14

The above four parameters are considered as the most important ones affecting the particle deposition behaviour. Bubble size determined directly the average transportation time of particles inside the bubble to the interfacial area. The density and size of particles directly affect the relaxation time of particles in gas flow. The surface tension is used in building the Weber number and thus has strong impact on the particle behaviour at the interface, determining whether a particle arriving the interface rebounds from the interface or penetration into water. The ranges of the four parameters indicated above cover well the conditions in pool scrubbing applications.

Fig. 11a–d show the remaining particle portion versus time. Here particle injection starts at $t = 0.0s$. It is well recognized, that all four parameters have strong effect on the decay behaviour of the remaining particle portion. The larger the particle size or the higher the particle density, the faster is the particle deposition due to larger relaxation time and increasing relative velocity between the particle and the gas phase.

The bubble size affects directly the average time for particles moving to the interfacial area. Thus, the smaller the bubble diameter, the shorter is the particle moving time and subsequently, the faster is the particle deposition. The surface tension of water has direct impact on the Weber number, defined in Eq. (29). The larger the surface tension, the smaller the Weber number. That means, the number of particles decreases, which impacts the interface and has Weber number exceed the critical Weber number. This leads to a decrease in the particle deposition and, thus, to a slower decay of remaining particle number.

$$We = \frac{4}{81}\frac{\rho_g(\rho_p - \rho_g)^2 g^2 d_p^4 D_B}{\mu^2 \sigma} \tag{29}$$

As discussed in Fig. 4, an exponential decay behaviour might be expected. Assuming that the decay behaviour of the remaining particles is presented with an exponential function:

$$N(t) = N_0 \cdot e^{-\alpha_p t} \tag{30}$$

From the above equation, it yields

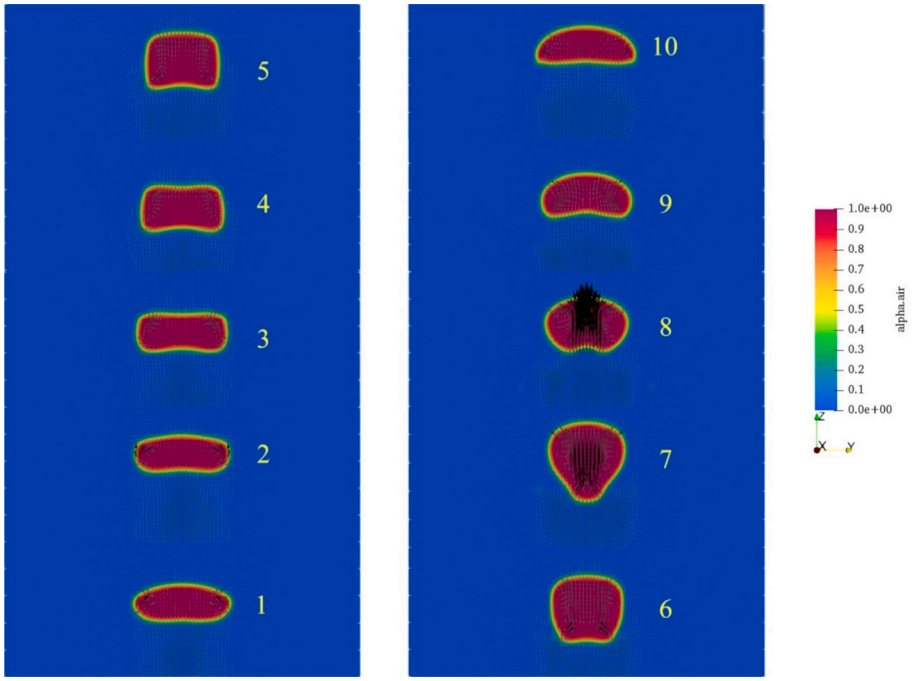

Fig. 10. Temporal evolution of bubble internal flow field (Mei and Cheng, 2022).

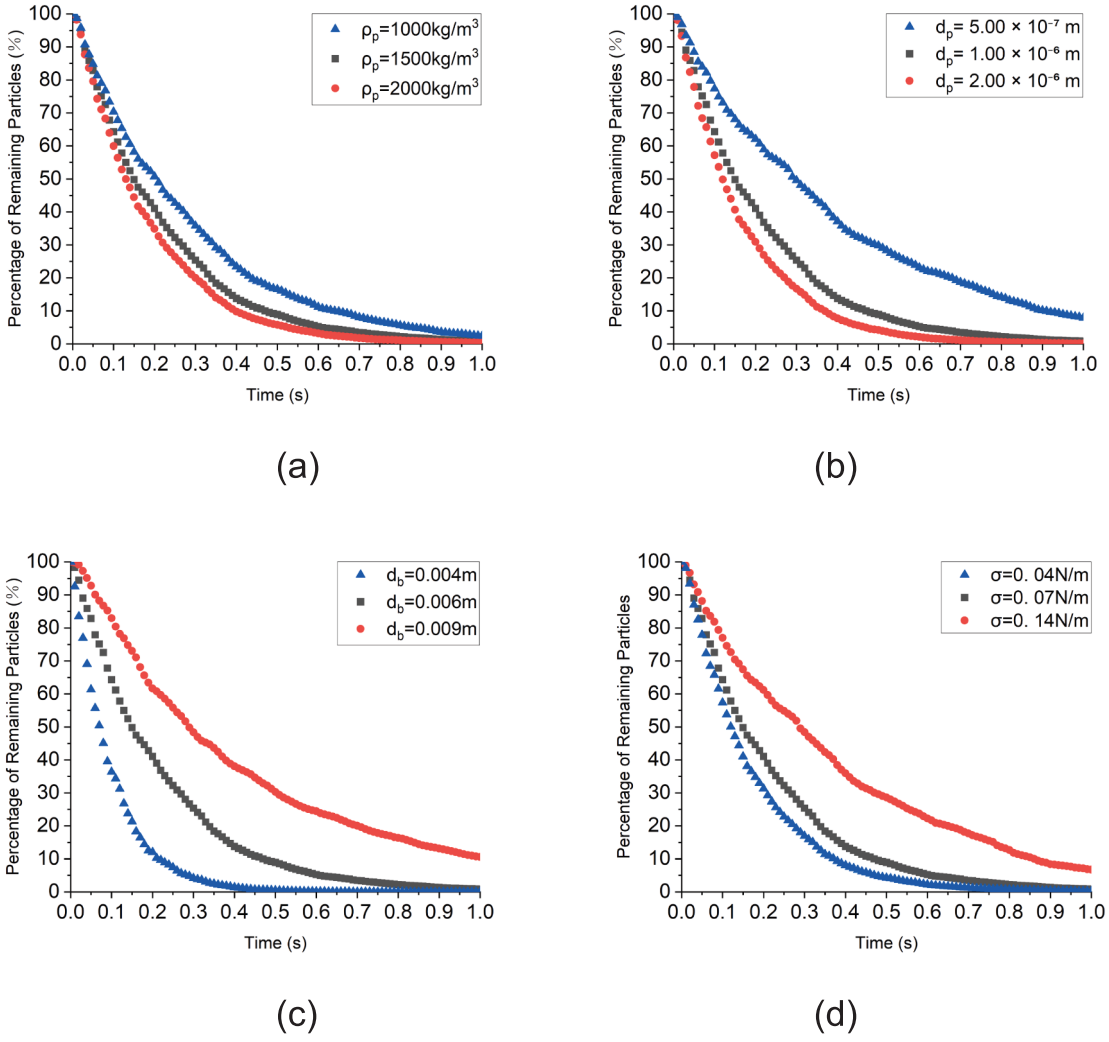

Fig. 11. Impact of physical parameters on particle remain during bubble transport.

$$ln\frac{N(t)}{N_0} = -\alpha_p t \tag{31}$$

Fig. 12a – 12d present the term $ln\frac{N(t)}{N_0}$ over time for the four various cases. In general, a good linear relationship between $ln\frac{N(t)}{N_0}$ and time is observed for all cases. This indicates the reasonable assumption of the exponential decay behaviour of the remaining particle portion with nearly constant values of the time constant, α_P in Eq. (30).

Surely the curves are not strictly linear lines. That means the decay constant α varies slightly versus time and is then expressed as:

$$\alpha_P(t) = -\frac{\ln\left(\frac{N(t)}{N_0}\right)}{t} \tag{32}$$

Table 1 summarizes the average values and the standard deviation of the decay constant, as defined as:

$$\overline{\alpha_P} = \frac{1}{\Delta t}\int_{t_1}^{t_2} \alpha_P(t)dt \tag{33}$$

$$STD = \sqrt{\frac{\sum_{k=1}^{M}(\alpha_k - \overline{\alpha_P})^2}{M}} \tag{34}$$

where M is total number of data points (population size).

The derive the average values and the standard deviation, numerical results in the time interval $(0.2s, 1.0s)$ were taken, which is divided into 80 time steps with each $0.01s$. It is assumed that after about 0.2 s, the effect of the initial injection condition is negligibly small. It can be seen from Table 1 that the standard deviation, i.e. the scattering from its average value, is small. This clearly confirms the assumption of the exponential decay behaviour and the feasibility of the new methodology in modeling the decontamination factor.

The average value of the decay constant depends strongly on all four parameters. The future task is to perform numerical analysis with more systematic variation of influencing parameters and to derive a model to describe the decay constant, if possible, based on dimensionless parameters.

4.2. Swarm flow and bubble residence time

The swarm flow behaviour was intensively investigated and documented in Kong and Cheng (2025). The main focus of this paper is put on the analysis of the bubble residence time. Following two parameters are taken into variation to study their effect on the bubble residence time, i. e.

- Gas injection volume flow rate, [L/s]: 0.1, 0.5, 1.5

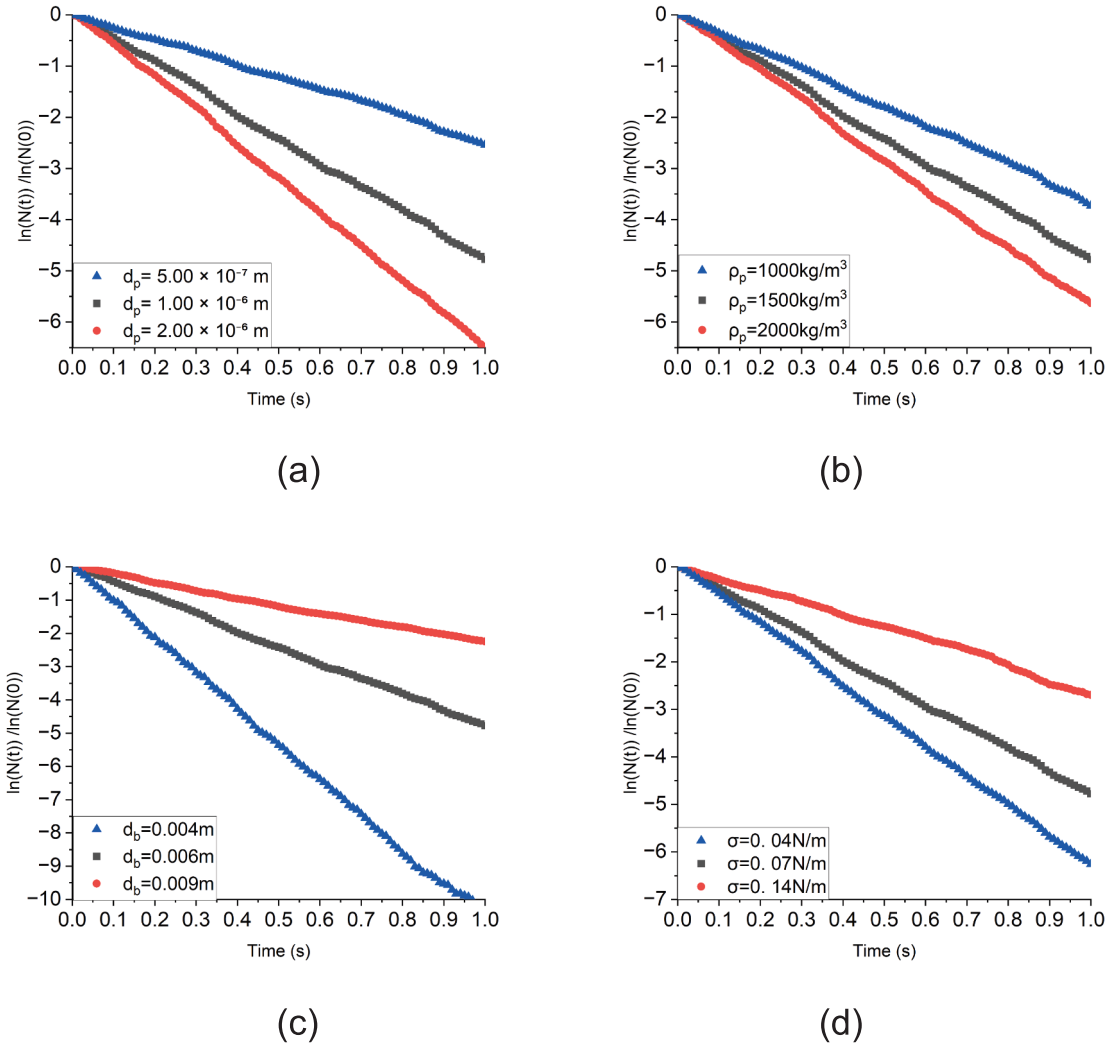

Fig. 12. Logarithmic decay of particle retention under varying parameters.

Table 1
Average value and standard deviation of decay constant.

D_B, mm	d_P, μm	ρ_P, mm	σ, N/m	$\overline{\alpha_P}$, 1/s	*STD*, 1/s
6.0	0.5	1500	0.07	2.43	0.07
6.0	1.0	1500	0.07	4.78	0.12
6.0	2.0	1500	0.07	6.35	0.19
6.0	1.0	1000	0.07	3.58	0.09
6.0	1.0	2000	0.07	5.65	0.15
4.0	1.0	1500	0.07	2.33	0.06
9.0	1.0	1500	0.07	10.63	0.12
6.0	1.0	1500	0.04	6.21	0.15
6.0	1.0	1500	0.14	2.54	0.10

- Bubble size, [mm]: 4, 6, 8

The above parameters belong to the most important ones affecting the bubble residence time. Bubble size determined bubbly dynamics and bubble rising velocity. It was found that gas injection rate affects directly the average bubble rising velocity, as indicated in Eq. (13).

To analyse the bubble residence time distribution, the reference case is simulated. For the operating conditions, the temperature of both water and air is 25 ℃, the bubble diameter is set as 4 mm and the volume flow rate of the injected air is 0.5 L/s. Through the Euler-Eulerian and

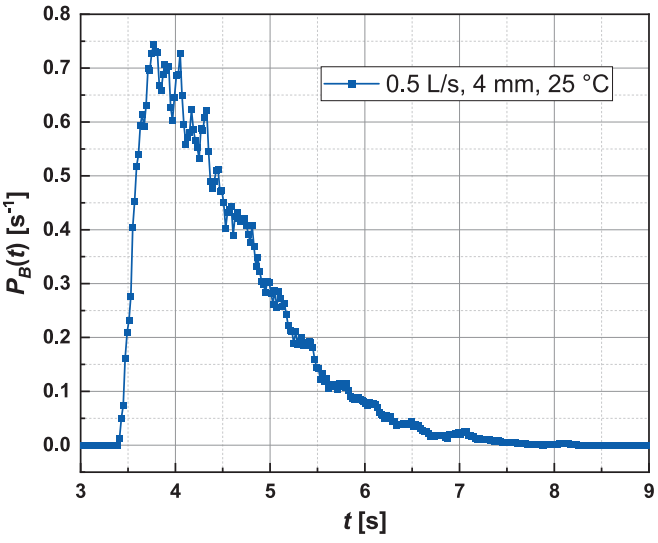

Fig. 13. $P_B(t)$ Curve for reference case.

Lagrangian approach, the two-fluid flow field was solved and individual bubble residence time was recorded. Fig. 13 shows the probability density function of the bubble removal P_B versus time. It is found that the bubble removal starts at time point $t_1 = 3.41s$, which the first bubble requires to reach the upper surface. After this time point, the bubble removal rate increases rapidly, reaches the maximum value at the point $t_2 = 3.77s$ and then decays slowly until all of the bubbles leave the water pool.

There is a portion of bubbles in the central part of the pool with a high rising speed. Their arrival at the upper surface results in the peak of the $P_B(t)$-curve. Bubbles from other parts of the pool with smaller velocities and are easily affected by natural circulation pattern would travel longer. Due to the decrease in the total number of bubbles, the removal rate decreases with the time.

For the bubble removal rate distribution, showed in simplified Fig. 14a, there are two important inflection points, i.e. t_1 and t_2. At t_1, bubble removal starts, representing the minimum bubble residence time and bubbles begin to leave the pool from this time point. Another is the peak of the bubble removal rate at t_2. The $P_B(t)$-curve can be divided into two parts by t_2. Generally, the bubble removal portion in the time interval (t_1, t_2) is shorter and the bubble removal portion is smaller. In the second stage, i.e. time interval (t_2, ∞), the $P_B(t)$-curve follows an exponential decay behaviour and, thus, is expressed as

$$P_B(t) = \alpha_2 e^{-\alpha_B(t-t_2)} \tag{35}$$

The integration of the $P_B(t)$-curve from t_2 to infinite is equal to the portion of bubbles removed in this time interval I:

$$\int_{t_2}^{\infty} \alpha_2 e^{-\alpha_B(t-t_2)} \mathrm{d}t = I \tag{36}$$

From the CFD results, the value t_2 and I can be directly determined. The coefficient α_2 is optimized by fitting the CFD results, as shown in Fig. 15. Thus, α_B can be easily obtained as

$$\alpha_B = \frac{\alpha_2}{I} \tag{37}$$

To take the bubble portion at the first stage (t_1, t_2) into account, the integration range is extended to $(t_2 - \tau_0, \infty)$, as shown in Fig. 14b, so that the integration yields

$$\int_{t_2-\tau_0}^{\infty} \alpha_2 e^{-\alpha_B(t-t_2)} \mathrm{d}t = 1 \tag{38}$$

From above two equations, τ_0 is then determined as

$$\tau_0 = \frac{1}{\alpha_B} ln\left(\frac{\alpha_B}{\alpha_2}\right) \tag{39}$$

The above analysis shows that as soon as both coefficients a_B and a_2 are determined according to the CFD results in the second stage, all other parameters can be easily obtained.

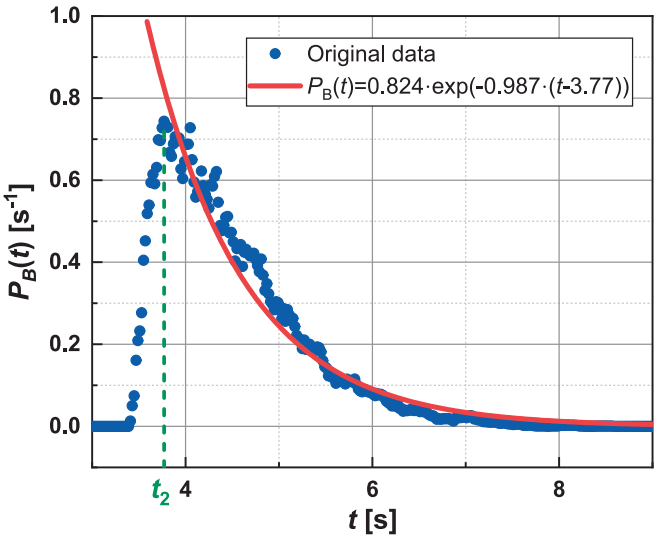

Fig. 15. Illustration of simulated results and fitting curve.

For the reference case, as shown in Fig. 13, the probability density function of bubble removal is generated and shown in Fig. 15. In this case, the coefficients α_2 and α_B are 0.824 and 0.987, respectively. The bubble removal peak occurs at time point $t_2 = 3.77s$. According to Eqs. (37) and (39), the portion of bubbles removed in the second stage is 83.5 %, and the effective starting time point $t_2 - \tau_0 = 3.59s$, just 0.18 s earlier than t_2.

Fig. 16 shows the effect of the bubble diameter (Fig. 16a and b) and of the gas volume flow rate (Fig. 16c and d) on the behaviour of the probability density function of bubble removal.

With the same procedure as indicated with Eqs. (35)–(39), the coefficients α_B and α_2, and the other parameters I, t_2 and τ_0 are obtained and summarized in Table 2. As the increase of volume flow rate, decay speed (α_B) increases, the removal peak point (t_2) moves towards a smaller value and the portion of bubble (I) leaves the water pool in the second stage changes irregularly. With the volume flow rate increases, local void fraction value also increases which leads to higher buoyancy and subsequently higher rising velocity. For case of 1.5 L/s, the wall effect becomes larger especially begins from the half of submerged height to the water surface due to large volume flow rate. Due to water circulation, more bubbles tend to move towards the wall, bubbles in the center rise slowly, and more bubbles leave the pool before the removal peak point.

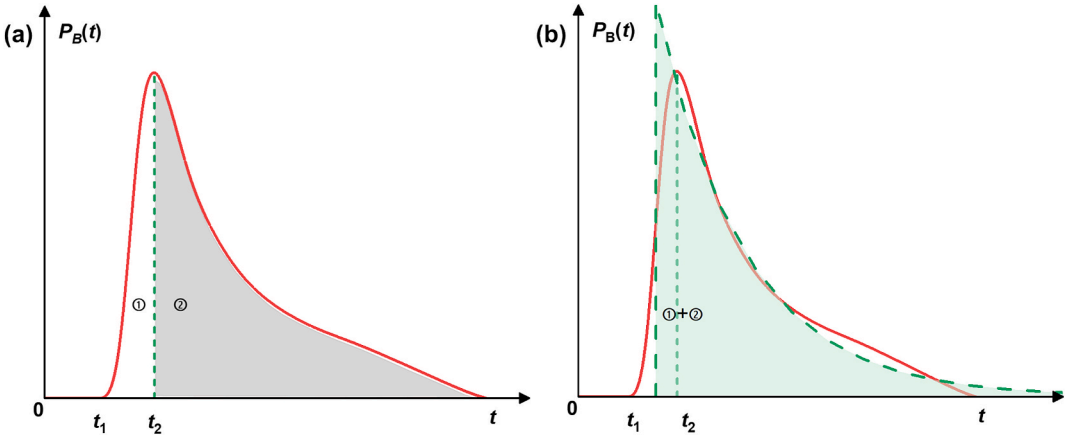

Fig. 14. Illustration of simplified $P_B(t)$ curve.

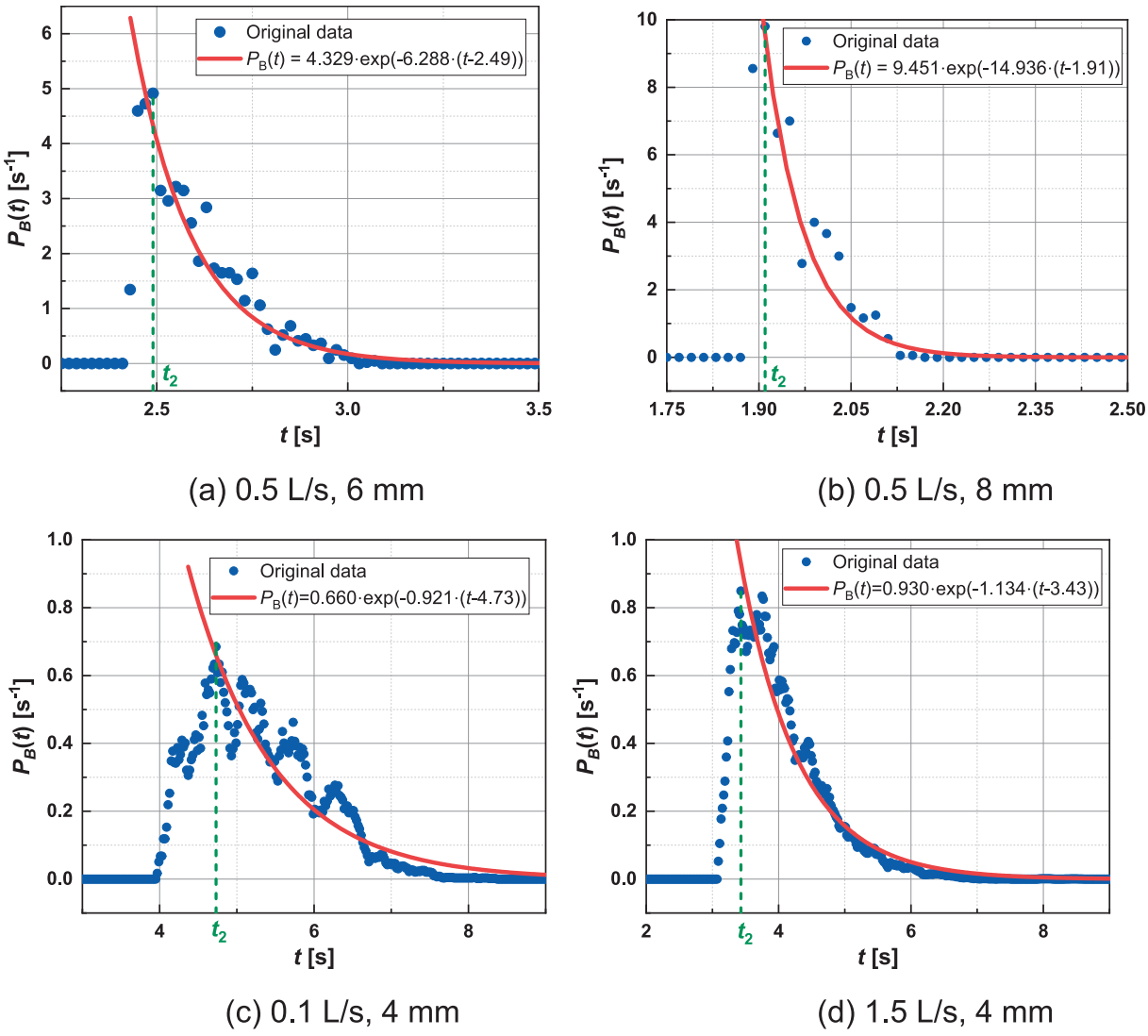

Fig. 16. Effect of bubble diameter and gas flow rate on the bubble removal.

Table 2
Fitting parameters of PDF for bubble removal.

Gas flow rate, L/s	D_B,mm	α_2, $1/s$	α_B, $1/s$	I, –	t_2, s	τ_0,s
0.5	4.0	0.824	0.987	0.835	3.77	0.18
0.5	6.0	4.329	6.288	0.688	2.49	0.06
0.5	8.0	9.451	14.936	0.633	1.91	0.03
0.1	4.0	0.660	0.921	0.717	4.73	0.36
1.5	4.0	0.930	1.133	0.821	3.43	0.17

As for the bubble diameter, α_B increases dramatically, I decreases, and t_2 also reduces significantly with the increase of bubble diameter. It is because larger diameter bubbles experience greater buoyancy, resulting in a higher rising velocity. Meanwhile, larger bubble tends to distribute in the center of flow due to lift force. Both cause most of bubbles to leave the pool more quickly and a larger portion of bubbles leaves in the first stage. The bubble diameter shows stronger effect on bubble removal because buoyancy force and lift force are proportion to the square of bubble diameter.

5. Summary

A reliable modelling of the decontamination factor plays a crucial role in the determination of the source terms of radioactive materials in the containment and affects the design of safety measures. In the widely applied aerosol retention code, conventional approaches for the modelling of the decontamination factor rely on the description of the particle deposition velocity. Due to the dynamic features of the bubble topology and bubble movement, the conventional approaches suffer from reliability and generality.

In this paper, a new approach was introduced to model the decontamination factor in swarm flow regime based on the statistical treatment of the residence time of bubbles in the liquid pool as well as the residence time of particles inside bubbles. The results achieved as far are summarized as below:

- An analytical equation, i.e. Eq. (18), was derived showing the relationship between the decontamination factor DF and both probability density functions $P_B(t)$ and $P_P(t)$, so that the task to determine the decontamination factor is converted to the task to model both probability density functions.
- Two different groups of CFD simulations were carried out to investigate the swarm bubble behaviour in water pool and the particle transportation inside bubbles, respectively. For the simulation of the swarm bubble behaviour, Euler-Eulerian method was used to determine the two-phase swarm flow field, whereas the Lagrangian Particle Tracking method was

selected for studying the bubble transportation and thus the bubble residence time.

- For single bubble simulation, the VOF method was applied to catch the interfacial surface of the bubble and the Lagrangian Particle Tracking method for the simulation of the particle transportation inside the bubble and, subsequently, the particle residence time.
- The numerical simulation of single bubble with particle transportation was carried out with different values of bubble size, particle size and particle density. It shows that the particle removal behaviour can be well described with an exponential decay function for all the cases, i.e.

$$P_P(t) = \alpha_P e^{-\alpha_P t}$$

The decay constant α_P is nearly constant for each case. The effect of various input parameters on the decay constant was physically explained.

- The numerical simulation of swarm flow with bubble tracking was performed with different gas injection flow rates and bubble diameters. A method was developed to overcome the effect of initial conditions. The behaviour of the bubble removal without the effect of the initial conditions was also well correlated with an exponential decay function, i.e.

$$P_B(t) = \begin{matrix} 0, & t < t_0 \\ \alpha_B e^{-\alpha_B (t-t_0)}, & t \geq t_0 \end{matrix}$$

The dependence of the decay constant on the input parameters was well explained.

- Combining the relationship between the decontamination factor and both probability density functions, i.e. Eq. (18), with the above two probability density functions, the decontamination factor can be easily obtained as

$$DF = \frac{\alpha_B + \alpha_P}{\alpha_B} e^{\alpha_P t_0}$$

As soon as models for the three parameters, α_B, α_P and t_0, are derived, the decontamination factor can be easily obtained. This confirms clearly the feasibility of the proposed new approach.

In the future, research needs are required in two aspects. At first, the numerical approach for the simulation of the particle transportation inside bubble requires experimental validation. For the development of models describing probability density functions of both bubble and particle removal behaviours, systematic numerical simulation with a large parameter range is necessary, to provide numerical data base for the model development.

CRediT authorship contribution statement

Xu Cheng: riting – original draft, Writing – review & editing, Formal analysis, Conceptualization. **Fanli Kong:** Writing – review & editing, Visualization, Software, Investigation, Data curation, Conceptualization. **Xing Chen:** Data curation, Investigation, Software, Visualization, Writing – review & editing.

Declaration of competing interest

The authors declare that they have no known competing financial interests or personal relationships that could have appeared to influence the work reported in this paper.

Acknowledgements

This work is funded by the German Federal Ministry for the Environment, Climate Action, Nature Conservation and Nuclear Safety (BMUKN) under grant number 1501652 based on a decision of the German Bundestag. The Ph.D. fellowship (No. 202208510049) from the China Scholarship Council (CSC) for the third author is appreciated.

Data availability

Data will be made available on request.

References

Abe, Y., Fujiwara, K., Saito, S., Yuasa, T., Kaneko, A., 2018. Bubble dynamics with aerosol during pool scrubbing. Nucl. Eng. Des. 337, 96–107. https://doi.org/10.1016/j.nucengdes.2018.06.017.

Bicer E., Cho H. K., & Honga S. J. (2021). CFD simulation of high inlet velocity air flow into a large tank at pool scrubbing conditions, Transactions of the Korean Nuclear Society Virtual Autumn Meeting.

Crank, J., 1979. The Mathematics of Diffusion. Oxford University Press, London, England.

Fujiwara, K., Nakamura, Y., Yoshida, K., Kaneko, A., & Abe, Y. (2020). Experimental investigation of particle decontamination efficiency in a single-bubble by pool scrubbing. International Conference on Nuclear Engineering, Vol. 83785, V003T13A010). American Society of Mechanical Engineers.

Fujiwara, K., Yoshida, K., Kaneko, A., Abe, Y., 2022. Experimental and numerical investigations of aerosol transportation phenomena from single bubbles. Int. J. Heat Mass Transf. 195, 123160. https://doi.org/10.1016/j.ijheatmasstransfer.2022.123.

Hänsch, S., Evdokimov, I., Schlegel, F., Lucas, D., 2021. A workflow for the sustainable development of closure models for bubbly flows. Chem. Eng. Sci. 244, 116807. https://doi.org/10.1016/j.ces.2021.116807.

Herranz, L. E., Sánchez, F. (2019). Critical assessment of the pool scrubbing database, 3rd Meeting of the IPRESCA Project, Frankfurt, Germany, June 27–28, 2019.

Herranz, L. E., Escudero, M. J., Peyrés, V., Polo, J., Lopez, J. (1996). Review and assessment of pool scrubbing models, CIEMAT, report No. CIEMAT–784, 1996.

Kong, F., Cheng, X., 2025. Analysis of swarm flow and bubble residence time under pool scrubbing conditions. Ann. Nucl. Energy 211, 110956. https://doi.org/10.1016/j.anucene.2024.110956.

Lee, Y. H., & Cho, Y. J. (2019). Results on benchmark problem for bubble hydrodynamics & preliminary sensitivity studies on size distribution of bubbles to decontamination factor via I-COSTA, 3rd Meeting of the IPRESCA Project, Frankfurt, Germany June 27–28, 2019.

Liao, Y., Li, J., Lucas, D., 2022. Investigation on pool-scrubbing hydrodynamics with VOF interface-capturing method. Nucl. Eng. Des. 390, 111713. https://doi.org/10.1016/j.nucengdes.2022.111713.

Mei, Z., Cheng, X., 2022. CFD simulation of instantaneous shape oscillation with rising velocity fluctuation for single bubble rising in water. Ann. Nucl. Energy 174, 109153. https://doi.org/10.1016/j.anucene.2022.109153.

Mei, Z., Cheng, X., 2023. Impact of bubble dynamics on aerosol transport based on CFD analysis. Prog. Nucl. Energy 161, 104723. https://doi.org/10.1016/j.pnucene.2023.104723.

Mei, Z., Cheng, X., 2024. Analysis of single bubble dynamics based on VOF method. Ann. Nucl. Energy 208, 110757. https://doi.org/10.1016/j.anucene.2024.110757.

Mei, Z., Kong, F., Cheng, X., 2022. Modeling of submicron particle transport based on VOF-LPT method. Chem. Eng. Sci. 264, 118168. https://doi.org/10.1016/j.ces.2022.118168.

Owczarski, P.C., Burk, K.W., 1991. SPARC-90: A code for calculating fission product capture in suppression pools. NUREG/CR- 5765, 1991. https://inis.iaea.org/collection/NCLCollectionStore/_Public/23/030/23030784.pdf.

Ramsdale, S. A., Guentay, S., & Friederichs, H. G. (1995). BUSCA-JUN91. Reference manual for the calculation of radionuclide scrubbing in water pools, GRS, 1995, ISBN 3923875665, 9873923875665.